J Mater Sci (2016) 51:4697–4708
DOI 10.1007/s10853-016-9787-9

Carbon fiber-reinforced epoxy filament-wound composite laminates exposed to hygrothermal conditioning

José Humberto S. Almeida Jr.[1] · **Samia D. B. Souza**[2] · **Edson C. Botelho**[2] · **Sandro C. Amico**[1]

Received: 14 November 2015 / Accepted: 25 January 2016 / Published online: 5 February 2016

Abstract This study focuses on the evaluation of the effect of hygrothermal conditioning on tensile, compressive, in-plane and interlaminar shear properties, and also on the viscoelastic characteristics of carbon fiber/epoxy laminates. Flat unidirectional laminates were manufactured by dry filament winding and cured under hot compression. The laminates were later exposed to hygrothermal conditioning in a chamber, following the recommendations of ASTM D5229M. All composite coupons were tested before and after conditioning. An analytical Fickian model was used to fit experimental data, showing very good estimates. Shear strength and modulus reduced to about 30 and 38 %, respectively. All specimens presented acceptable failure modes; shear specimens failed at the gage section with delaminations and fiber/matrix debonding, whereas short beam specimens failed via delaminations at the specimen mid-plane. Moisture penetration through the carbon/epoxy surface lead to interfacial debonding and matrix plasticization. Puck's failure envelope accurately predicted failure under compressive and shear loading.

✉ José Humberto S. Almeida Jr.
jhsajunior@globomail.com

[1] PPGE3M, Federal University of Rio Grande do Sul, Av. Bento Gonçalves 9500, Porto Alegre, RS 91501-970, Brazil

[2] Department of Materials and Technology, Universidade Estadual Paulista (UNESP), Av. Ariberto Pereira da Cunha 333, Guaratinguetá, SP 12516-410, Brazil

Introduction

Carbon fiber-reinforced epoxy composites are commonly used in applications with high structural demand, such as marine, aeronautical, and aerospace sectors [1]. Among the manufacturing processes available for advanced polymer composites, filament winding (FW) stands out, being able to produce from flat laminates to elbows and curved-surface structures. The high fiber volumetric fraction and precision in angle deposition, along with the use of a tensioned and continuous reinforcement are the main features of FW.

The oil and gas sector, in particular, is increasingly replacing metallic-based structures with composites based on the need to increase payload in marine structures by reducing weight and increasing corrosion resistance. Indeed, pipelines, subsea systems, and submersible structures operate under aggressive environments, which modify the mechanical response of the composite, decreasing damage tolerance and sometimes leading to premature failure [2].

Prediction of failure and damage in composites is typically complex mainly due to their orthotropic characteristic, and this becomes even more complex when the material is under extreme weathering conditions. When under these environments, composites can absorb moisture, which affects their long-term durability and properties [3]. Since high-performance carbon fibers absorb virtually no moisture, absorption is largely matrix-dominated [4], suggesting that matrix-dominated failure mechanisms will be more significantly affected. Also, if the matrix content is high or if a fiber more prone to absorption is being used (e.g., polyaramid), the greater the expected water absorption.

Moisture permeation is dominated by diffusion, capillarity, and/or transport by micro-cracks, and the rate of

moisture uptake varies with the type of matrix, fiber orientation, water temperature, moisture [5], and fiber content (V_f). Moisture wicking can promote changes in mechanical, thermo-mechanical, and thermo-physical characteristics of the matrix by plasticization, swelling, cracking, and hydrolysis, and it can also degrade fiber-matrix bonding [3, 6]. When combined with high temperatures, it may induce irreversible structural changes in the polymer network. The extent of damage may change swelling, since cracking and blistering cause higher uptake, whereas the leaching of small molecule components results in gradual decrease in weight gain [7].

Ultraviolet radiation (UV) can also degrade the matrix and cause irreversible structural changes. UV radiation can trigger photolytic, photo-oxidative, and thermo-oxidative reactions within the matrix. Degradation can cause from simple discoloration to substantial loss of mechanical properties as a result of C–C polymer chain scission [8] due to photo-oxidation [9]. Another effect is the cross-linking, which restricts molecular mobility and reduces the ability of the material to accommodate externally applied strain [10].

Marine structures sometimes operate under combined UV and seawater influence both being detrimental to polymeric composites. Botelho et al. [11] evaluated the effect of different hygrothermal conditionings on the shear behavior of carbon/epoxy composites and Mouzakis et al. [9] studied accelerated environmental aging of glass/polyester composites, reporting a significant decrease in compression and shear strength. Thus, this paper addresses the effect of environmental conditioning (accelerated water immersion) on the tensile, compressive, in-plane shear, and viscoelastic properties of flat filament-wound carbon fiber/epoxy laminates.

Experimental

Materials and manufacturing

Carbon fiber/epoxy prepreg tow (towpreg) from TCR Composites, with Toray T700-12 K-50C carbon fiber and UF3369 epoxy resin system, was used in this work. The flat laminates were manufactured using a rectangular stainless steel mandrel (327 × 228 × 12 mm^3) and a KUKA robot KR 140 L100 with control and peripheral devices from MFTech, with an achievable tolerance in the winding angle lower than 0.5 %. Hoop flat laminates were produced on the designed mandrel, as presented in Fig. 1. Two simultaneous rovings (towpregs) were used to produce the laminates. The towpregs were then wound onto the mandrel. After winding, a polyester-based shrink tape was used to wrap and help consolidating the laminate during the curing process that followed. The tape begins to shrink around 70 °C and reaches a maximum shrink force at 150 °C. This aids ply compaction and the elimination of voids, yielding a resin-rich part surface.

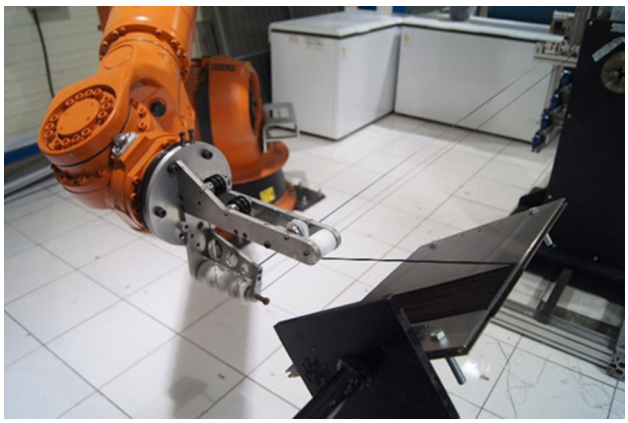

Fig. 1 Manufacturing of a flat unidirectional laminate by filament winding

The laminates were cured by hot compression under six ton for 4 h at 130 °C. The final fiber volume fraction was ≈72 % (measured by acid digestion following ASTM D3171-11) and mean ply thickness was 0.35 mm in the 4-layer laminate (overall thickness of 1.40 mm).

Weathering

The carbon fiber/epoxy specimens were exposed to a combination of temperature and humidity for 60 days at 80 °C under a relative humidity of 90 % inside a hygrothermal climatic chamber Marconi, model MA835/UR. The hygrothermal exposure was carried out following the recommendations of ASTM D5229M-14. The samples went through a drying procedure to guarantee that they were dry and in mass equilibrium before aging, preventing that initial and atmosphere humidity affected water uptake values [1, 12]. The drying cycle can be summarized as follows: the sample was weighed, placed in an oven at 110 °C for 24 h, removed from the oven and placed in a desiccator, weighed again, and placed in an oven at 110 °C for 3 h. These stages were repeated until the specimen reached mass equilibrium, and only then, they were placed in the hygrothermal chamber for 60 days at 80 °C and 90 % humidity. The sample mass was periodically monitored, and moisture absorption (M) was calculated using $M = (M_w - M_d)/M_d$, where M_w and M_d are the wet and dry masses, respectively.

In order to better understand moisture absorption and diffusion response of the composites herein analyzed, Fick's analytical model [13], shown in Eq. (1), was applied to the data.

$$M_t = M_\infty \left\{ 1 - \exp\left[-7.3 \left(\frac{Dt}{h^2} \right)^{0.75} \right] \right\} \quad (1)$$

where M_t is water uptake at a particular time t, M_∞ is the mass at a quasi-equilibrium state, D is the diffusion coefficient, and H is the specimen thickness. The diffusion coefficient is calculated from the absorption curve, as shown in Eq. (2):

$$D = \pi \left(\frac{h}{4M_\infty} \right)^2 \left(\frac{M_2 - M_1}{\sqrt{t_2} - \sqrt{t_1}} \right)^2 \quad (2)$$

where the subscripts in M and t refer to a particular mass and time, respectively.

Characterization

The unidirectional composites were cut longitudinally and transversely to the fiber direction. Mechanical testing was carried out using an Instron 3382 universal testing machine, with 100 and 5 kN load cells, in samples before and after the environmental conditioning. The tests were:

- *Tensile* This test was performed at a cross-head speed of 2 mm/min in five tabbed coupons of controlled geometry dimensions following ASTM D3039-14. From this test, the elastic moduli, tensile strengths, and Poisson's ratio were obtained. Two extensometers, one longitudinal and another transversal, were coupled to the specimens for testing and later removed just prior to rupture.
- *Compression* The compressive strength was obtained with the combined loading compression test according to ASTM D6641-09 in five tabbed specimens. The size of the specimens was 140 × 12 × 1.4 mm^3, the gage length was 12 mm, and the speed rate was 1.3 mm/min.
- *In-plane shear* The V-notched rail shear method (ASTM D7078-12) test was chosen. The specimen (dimensions: 76 × 56 × 2.8 mm^3) was centrally V-notched on both sides. The notch angle is 90° and the radius is 1.3 mm. Cross-head speed was 1.5 mm/min and the shear modulus was determined on six samples using a strain gage rosette aligned at ± 45° at the mid-section of the sample (as seen in Fig. 2).
- *Short beam* Interlaminar shear strength was evaluated through short beam tests, following ASTM D2344-13, using a span-to-depth thickness (*s:t*) ratio of 4:1. Length and width of the samples followed the recommendations of the standard (6 × t and 2 × t, respectively).
- *Dynamic mechanical analysis* (*DMA*) DMA was used to evaluate the glass transition temperature (T_g) of the polymeric matrix. Analysis was carried out in a TA Instruments 2980 DMA Dynamic Mechanical Analyzer under single-cantilever bending mode at 1 Hz frequency, for a maximum displacement of 10 mm, under N_2 atmosphere, with a heating rate of 3 °C/min, on 20 × 10 × 2.8 mm^3 specimens.
- *Failure analysis* Fractographic studies were carried out using optical micrographs in a Carl Zeiss Axio scope and scanning electron microscopy (SEM), in a Phenom ProX equipment.

Fig. 2 V-notched shear test with a bonded rosette

Failure envelope

Classical failure criteria (Maximum stress, Tsai-Wu [14], Tsai-Hill [15], Hashin [16], Christensen [17], and Puck [18]) were used to predict failure envelope in the σ_{22}–τ_{12} plane, assuming the stress in fiber direction being σ_1, stress in the transverse σ_2, and τ_{12} the shear stress.

Results and discussion

Moisture uptake

Figure 3 presents the mass uptake for the 0° unidirectional carbon fiber/epoxy coupons (average of five coupons) after hygrothermal conditioning. Water uptake is influenced by (i) the hydrophilic character of the matrix and fibers, (ii) fiber/matrix adhesion, (iii) micro-cracks, and (iv) voids. The resin network controls water uptake and, in turn, the absorption of water influences the network. Formation of voids and micro-cracks is induced by water absorption, becoming more important as the saturation level increases [13].

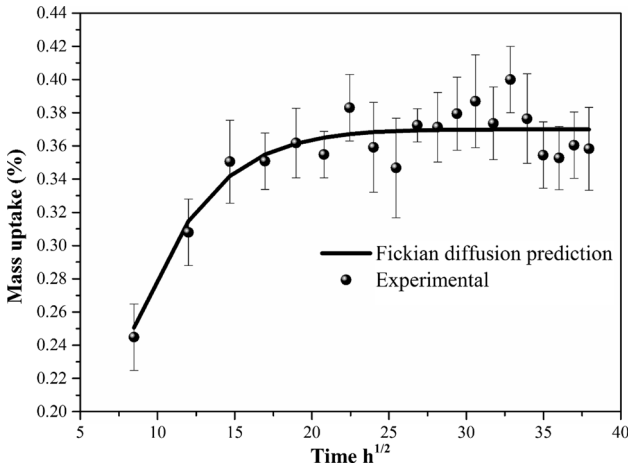

Fig. 3 Mass gain obtained from experimental measurements and Fickian diffusion prediction

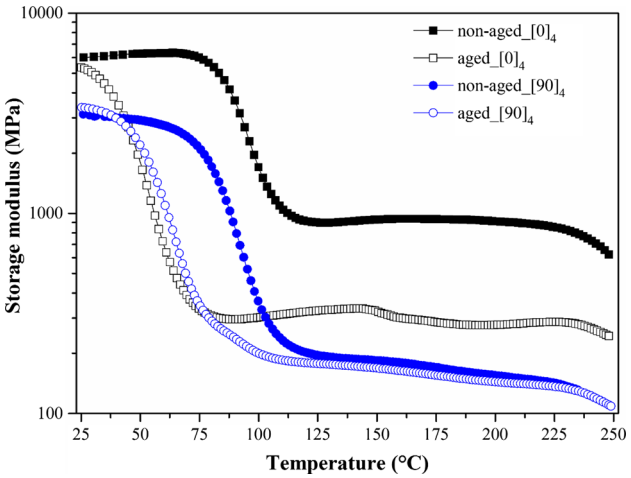

Fig. 4 Storage modulus of the unconditioned and weathered specimens

Hot/wet environment accelerates the deterioration process of an epoxy-based composite. Reproducibility of the experimental data is well predicted by the Fickian model, both experimental and analytical data being representative in terms of water content of the material. The initial stage till pseudo-equilibrium is typical of a thermally activated Fickian response, whereas, at longer times, the uptake occurs at a lower rate mainly due to a combination of mechanisms such as relaxation of the glassy epoxy network, filling of micro-voids, and debonded zones with water by wicking [19]. Thus, moisture absorption is expected to take place via diffusion.

Kinetics of the diffusion process depends on temperature and relative moisture absorption. The higher the relative moisture absorption, the greater the absorption rate. Water saturation ($\approx$0.37 %) reached at around 30 days, and maximum mass uptake, about 0.40 %, was noticed after 42 days of conditioning, both are typical of epoxy resins. Moreover, mass uptake values were relatively low compared to literature data for the same matrix and fiber [8, 12, 13, 20], which can be justified by the high fiber volumetric fraction and good compaction of the layers.

Viscoelastic properties

Figure 4 shows the storage modulus (E') for the unconditioned and conditioned composites studied. As expected, storage modulus for 0° specimens was higher than for 90° in all states (glassy, elastomeric, and rubbery). This particular DMA analysis was performed under bending mode, which is markedly dependent on fiber orientation, which is stiffer for fibers aligned along the length of the specimen. Unconditioned specimens showed higher storage modulus compared to the weathered ones, which is related to the plasticizing effect promoted by moisture uptake.

The aged composites showed similar behavior at the glassy state, perhaps due to a post-curing that may take place during aging. The relatively high temperatures involved, although not severe enough to break chemical bonds of the polymer [8], may contribute to the appearance of free radicals in the epoxy molecules, leading to further cross-linking [9].

The loss modulus (E'') is related to energy dissipation in the material, and composites with poor interfacial bonding are prone to dissipate more energy. Some specimens presented a more flattened loss peak, where the hygrothermally conditioned specimens had lower loss modulus, as seen in Fig. 5. Analysis of the curves shows that the behavior was more affected by fiber orientation than by weathering, and the specimens with fibers at 0° presented much higher peaks. For the 90° specimens, the aged laminate dissipated slightly less energy. This can be attributed

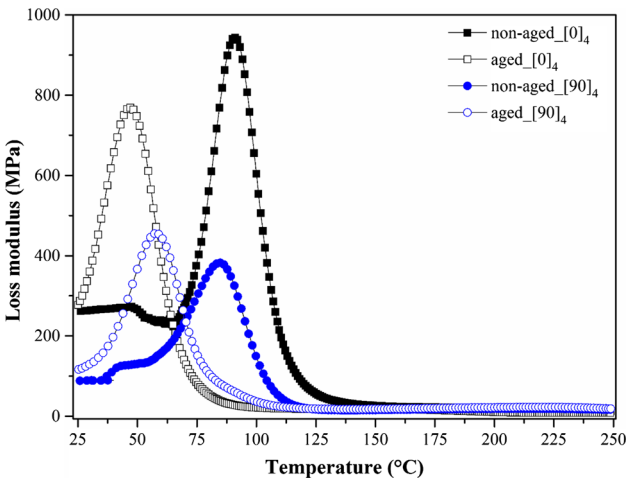

Fig. 5 Loss modulus of the unconditioned and weathered composites

to the inhibition of relaxation processes in the composites, decreasing mobility at the fiber/matrix interface.

Tan δ curves are shown in Fig. 6. The unconditioned specimens showed similar temperature at the peak (i.e., T_g), and the conditioned samples showed similar and lower T_g values. The weathering effect on the composites is more clearly observed in this figure, i.e., the conditioned specimens show larger areas under the peak and lower T_g, suggesting matrix degradation [21].

Table 1 presents the T_g extracted from (i) intersection between the extrapolation of the elastomeric plateau and the glass state from the storage modulus curve, (ii) the loss modulus peak, and (iii) the tan δ peak. The unconditioned 0^o specimen showed the highest T_g, but the aged 0^o specimen showed the lowest value in all methods; thus this specimen is more damaged by aging, confirming that fiber orientation has little effect on the glass transition of the polymer.

Mechanical properties

Figure 7 presents the typical load versus displacement curves for all samples. Based on the mean results of five specimens with acceptable failure, conditioning reduced tensile strength of the laminates from 1409 ± 131 to 1091 ± 114 MPa, around 29 %. Although the 0°-oriented specimens presented a slight flattening near the failure, these specimens presented a brittle behavior, typical for this type of loading/sample.

Figure 7 also shows tensile behavior of the 90^o-oriented composites. Brittle behavior was dominant for both non-aged_$[90]_4$ and aged_$[90]_4$ specimens and the ultimate load was significantly low compared to longitudinally oriented laminates. In addition, aging reduced in about 25 % their tensile strength.

Even though the load versus displacement curves somewhat differ for the various longitudinally oriented specimens, all coupons showed similar failure mode (see Fig. 8a), with a sudden failure of the fibers. All 10 fractures (five for aged and five non-aged) were characterized as explosive gage middle. The failure mode for all 90^o samples, conditioned and non-conditioned, was also similar—lateral gage middle failure (see Fig. 8a), with only one lateral at the top tab failure. Since the optical micrographs indicated a good quality laminate, essentially free of voids (Fig. 8c, d), a weakened fiber/matrix interface may have appeared after aging (Fig. 8d), corroborated by some resin-rich areas due to water uptake and more brittle fracture at the carbon/epoxy interface, which reduced tensile strength. Furthermore, Fig. 8d suggests that broken fibers tend to initiate failure in adjacent fibers.

Stress versus strain data for the tensile testing of non-aged and aged composites are shown in Fig. 9. The final properties may be summarized as follows: (i) Non-aged: $E_{1,t} = 129.8 \pm 5.6$ GPa and $E_{2,t} = 9.1 \pm 0.5$ GPa, and

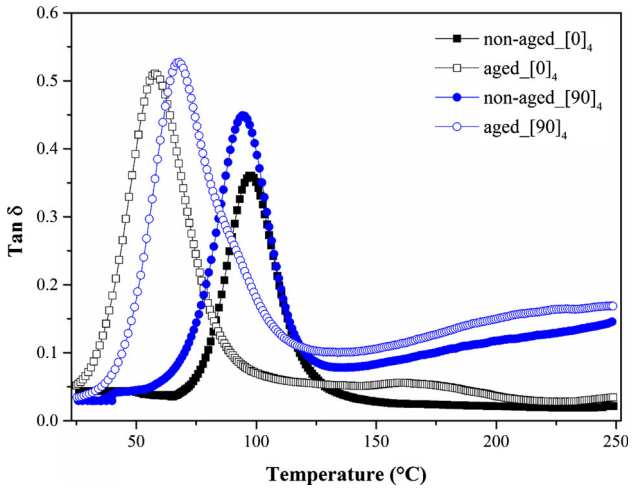

Fig. 6 Tan delta of the unconditioned and weathered specimens

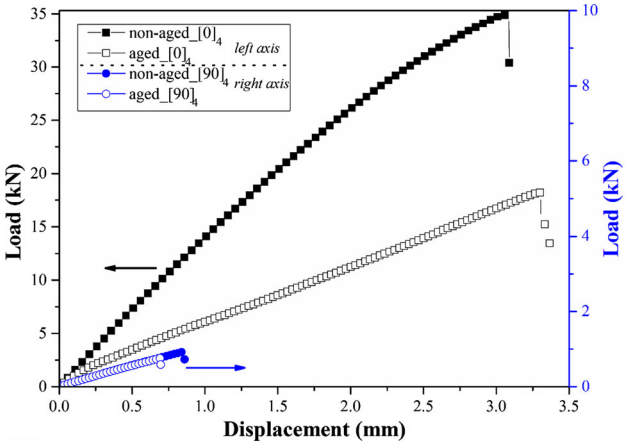

Fig. 7 Typical load × displacement tensile curves for the studied families of unidirectional laminates

Table 1 T_g determined by different methods

Specimen	T_g (°C) from onset E' drop	T_g (°C) from E'' peak	T_g (°C) from tan δ peak
Non-aged_$[0]_4$	78.3	91.0	98.1
Aged_$[0]_4$	35.2	47.7	57.9
Non-aged_$[90]_4$	68.9	84.8	94.7
Aged_$[90]_4$	44.7	57.8	67.4

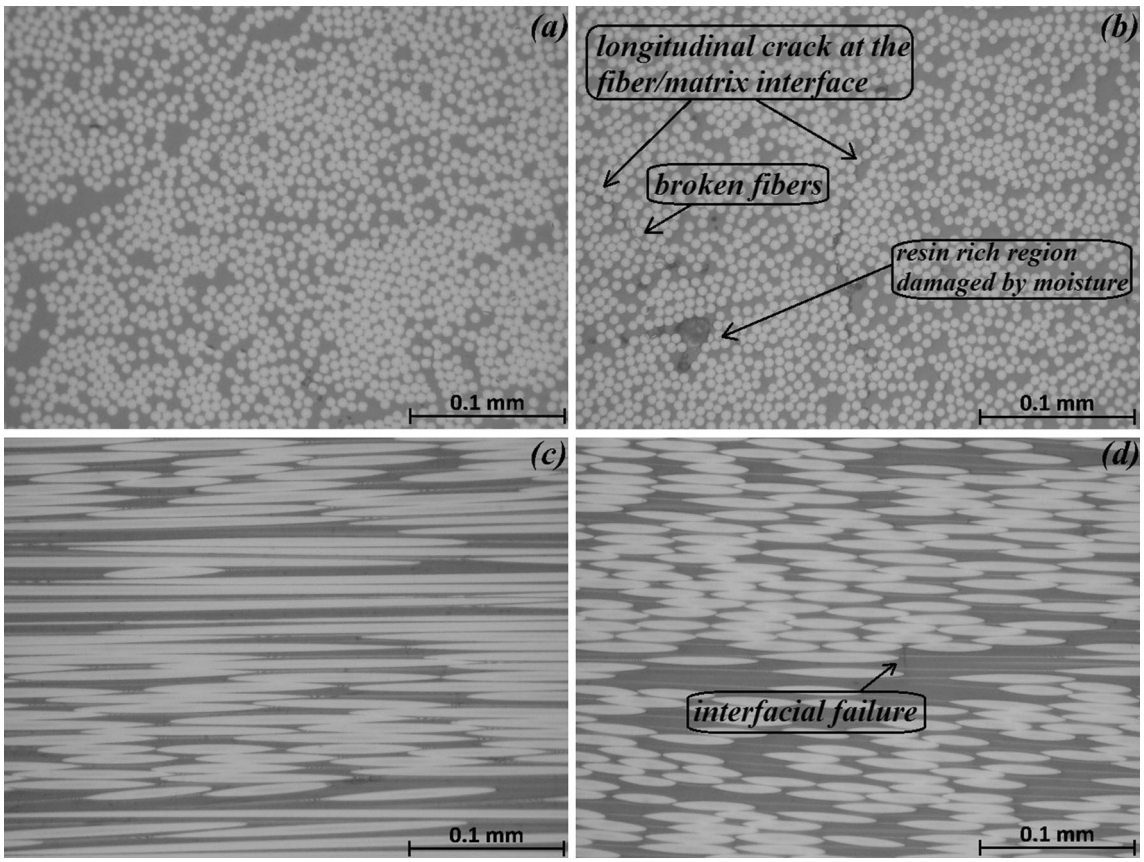

Fig. 8 Optical micrographs are shown for the fractured non-aged_$[0]_4$ **a**, aged_$[0]_4$ **b**, non-aged_$[90]_4$ **c**, aged_$[90]_4$ **d** tensile coupons

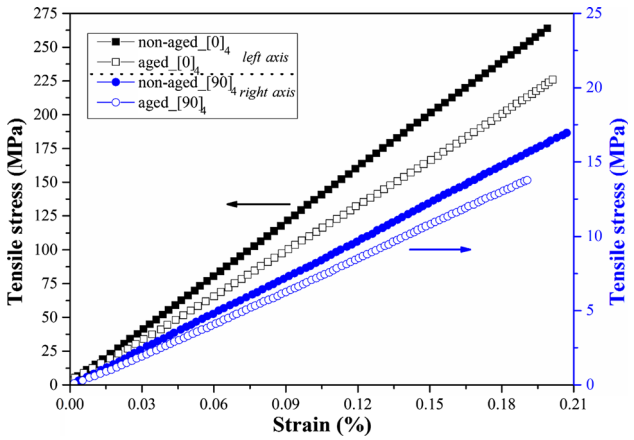

Fig. 9 Stress × strain profile plots for all coupons measured by longitudinal and transversal analogical extensometers

(ii) Aged: $E_{1,t} = 119.7 \pm 4.1$ GPa and $E_{2,t} = 6.3 \pm 0.8$ GPa. A more significant drop in E_2 may be justified considering that this property is more influenced by the characteristics of the matrix, which is more severely affected under hygrothermal aging.

Figure 10 presents the longitudinal (ε_1) and transverse (ε_2) ultimate strains of the composites. For the 0° laminates, a more linear shape of the curves is noted, since ε_1 is much higher than ε_2, leading to a more consistent relationship between strains. The measured major Poisson's ratio (v_{12}) was 0.31 ± 0.02 for the non-aged_$[0]_4$ coupon. For unidirectional laminates, v_{21} is not easy to measure because of the very low strain magnitude. Nevertheless, the experimentally measured v_{21} was 0.020 ± 0.001, very close to that estimated through the correlation $v_{21} = v_{12} \times E_2/E_1$, i.e., 0.021.

Compressive results for all samples are presented in Fig. 11. A non-linear behavior was noticed for non-aged and aged specimens, mainly attributed to micro-buckling caused by delaminations, as suggested by the tiny discontinuities along the testing direction, mainly for non-aged_$[0]_4$ and non-aged_$[90]_4$ coupons. It is important to bear in mind that the compressive load is transmitted though shear from the fixture to the specimen, and shear has a significant influence up to around 60 % of the test, when a purer compression stress state is achieved. The specimen with longitudinally aligned fibers is more affected by aging since the decrease in matrix modulus favors micro-buckling. On the other hand, the 90° specimens are less affected by aging since, under compressive loading, failure occurs at the transversally oriented carbon fiber.

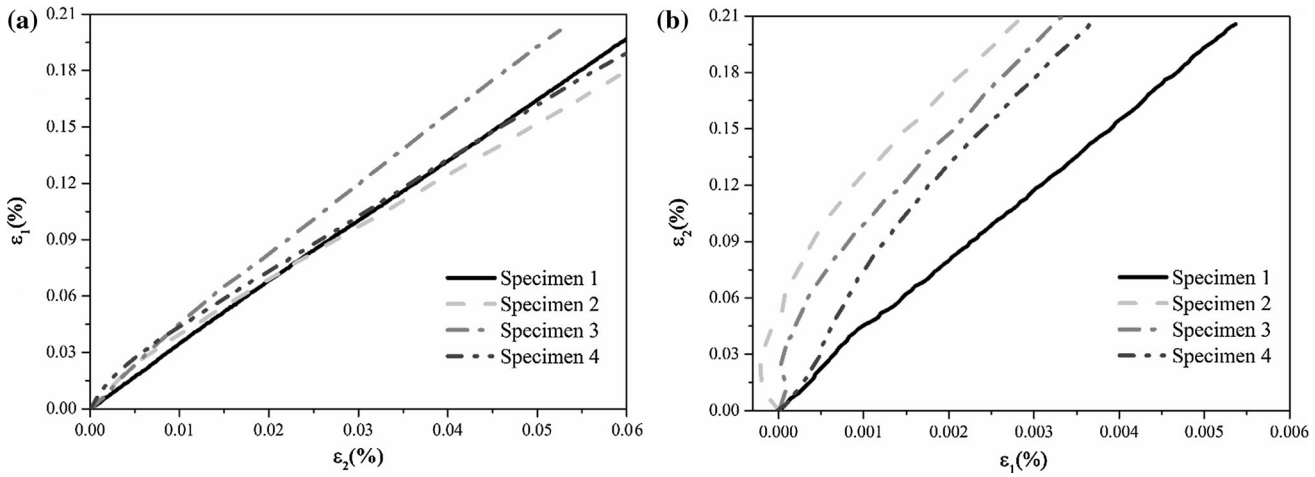

Fig. 10 Longitudinal × transversal strains for determining the major (**a**) and minor (**b**) Poisson's ratio for non-aged_$[0]_4$ **a** and non-aged_$[90]_4$ **b** tensile specimens

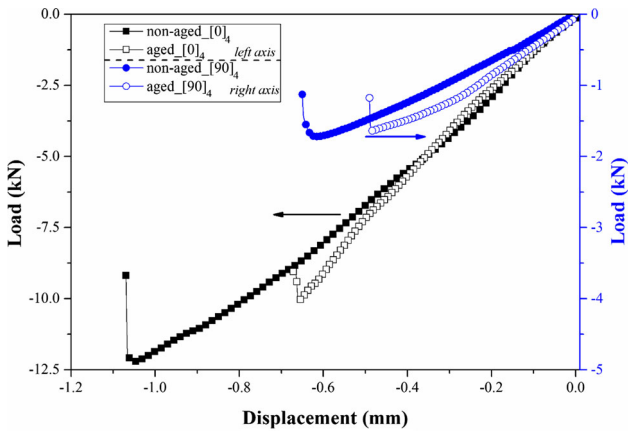

Fig. 11 Typical load × displacement compressive curves for all specimens studied

Unlike tensile failure, the compression fracture surfaces are not usually normal to the loading direction, but slightly angled, since compression leads to a small degree of in-plane shear during fracture [22]. Since the laminate with compression fracture is still able to carry load after ultimate failure, minor damages such as longitudinal splits and delaminations may occur [23]. These characteristics can be confirmed in Fig. 12, highlighted as an implication of the fractured non-aged_$[0]_4$ specimen. The morphology of the failure points that band of fibers fail at similar lengths, leading to the formation of kinking bands.

Figure 13 displays the shear stress × displacement curves obtained in the V-notched rail test method. These plots show typical shear behavior, and after around 50 % of the test, most specimens started to delaminate, followed by horizontal

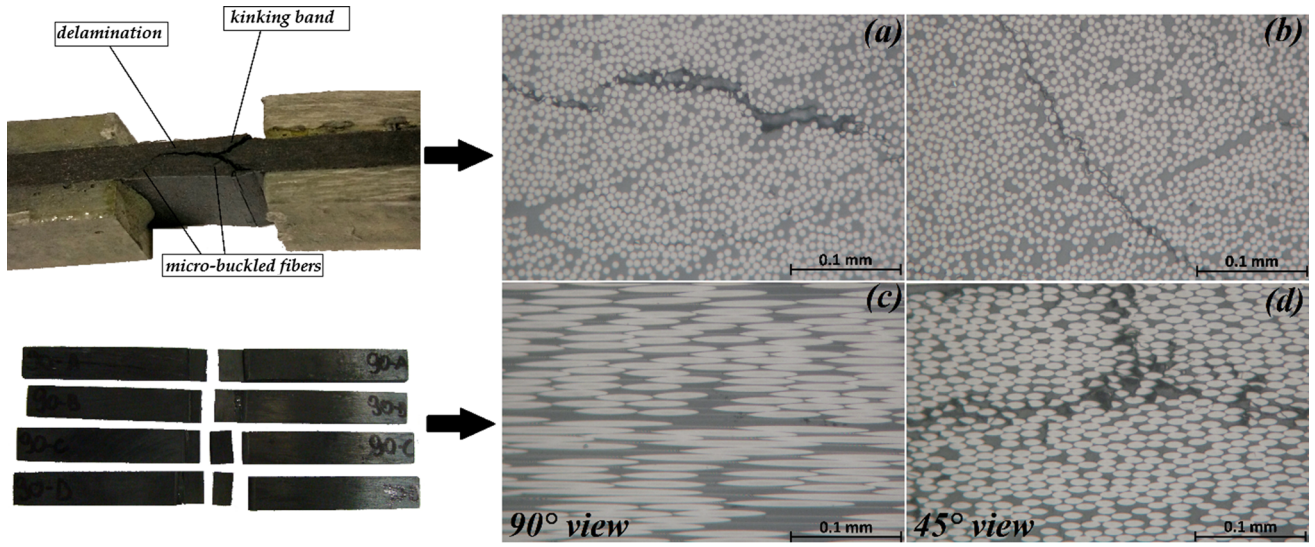

Fig. 12 Optical micrographs for the fractured non-aged_$[0]_4$ **a**, aged_$[0]_4$ **b**, non-aged_$[90]_4$ **c**, aged_$[90]_4$ **d** compressive coupons

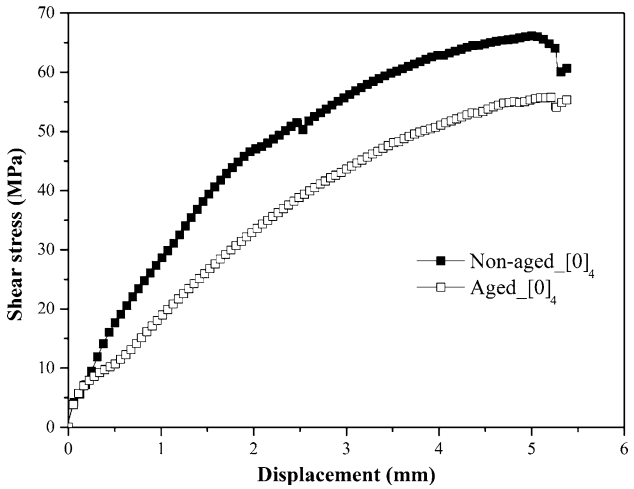

Fig. 13 Typical shear stress × displacement curve profiles for non-aged **a** and aged **b** coupons

micro-cracks at the gage area. Good compaction of the laminates manufactured by FW can be inferred from this graph.

The breaking load was c.a. 40 % lower for conditioned specimens, indicating a strong aging effect since this is also a matrix-dominated property. The water absorbed by epoxy-based composites causes reversible plasticization of the matrix, and the combined moisture and temperature action yields dimensional changes and induces stresses that are detrimental to the fiber–matrix interface.

The shear stress × strain profile curves are presented in Fig. 14. For both non-conditioned (Fig. 14a) and conditioned (Fig. 14b) specimens, the curve profiles were very linear, with $R^2 > 0.99$ for all specimens. Shear modulus reduced after aging, from $G_{12} = 5.44 \pm 0.48$ GPa to $G_{12} = 3.89 \pm 0.19$ GPa.

The failure mode of all specimens (Fig. 15) was very similar, being characterized as horizontal cracking between the notches (HGN) and multi-mode cracking at the gage section between the notches (MGN). Crack started horizontally close to the top notch, probably due to some stress concentration caused by machining of the notches. Later, many delamination cracks perpendicular to the loading direction appeared at the mid-section of the specimen. Representative micrographs of the notch areas of 0° specimens are highlighted in Fig. 15. Matrix cracking and fiber/matrix debonding dominated the failure mode for unconditioned specimens, whereas large delaminations initiated from hygrothermally damaged resin-rich regions dominated for conditioned specimens. These cracks originated primarily from fiber splitting at a particular lamina and interlaminar shear at the carbon/epoxy interface. In parallel, as aging deteriorates the epoxy matrix, it decreases the overall interfacial strength of the laminate.

Short beam strength (SBS) results are shown in Fig. 16. SBS values for 0° samples were 69.9 ± 1.1 and 49.5 ± 1.3 MPa for non-aged and aged, respectively. For transversally aligned fibers, SBS reduced from 12.6 ± 0.6 to 7.4 ± 0.7 MPa for non-aged and aged laminates, respectively. Short beam is one of the most recommended tests to investigate fiber/matrix interface and, from these results, it is clear that aging damages the interface, reducing interfacial strength in about 41 and 70 % for non-aged_$[0]_4$ and non-aged_$[90]_4$, respectively.

Typical load versus displacement curves suggest that the 0° coupons failed by shear, presenting a non-linear behavior followed by discontinuities along the test, typical of delaminations and interlaminar fractures. On the other hand, the 90° samples presented a more linear behavior with brittle fracture, suggesting a strong influence of tensile load in the test. As in Almeida Jr. et al. [24], the SBS is strongly dependent on fiber orientation and it decreases from 0° to 90°.

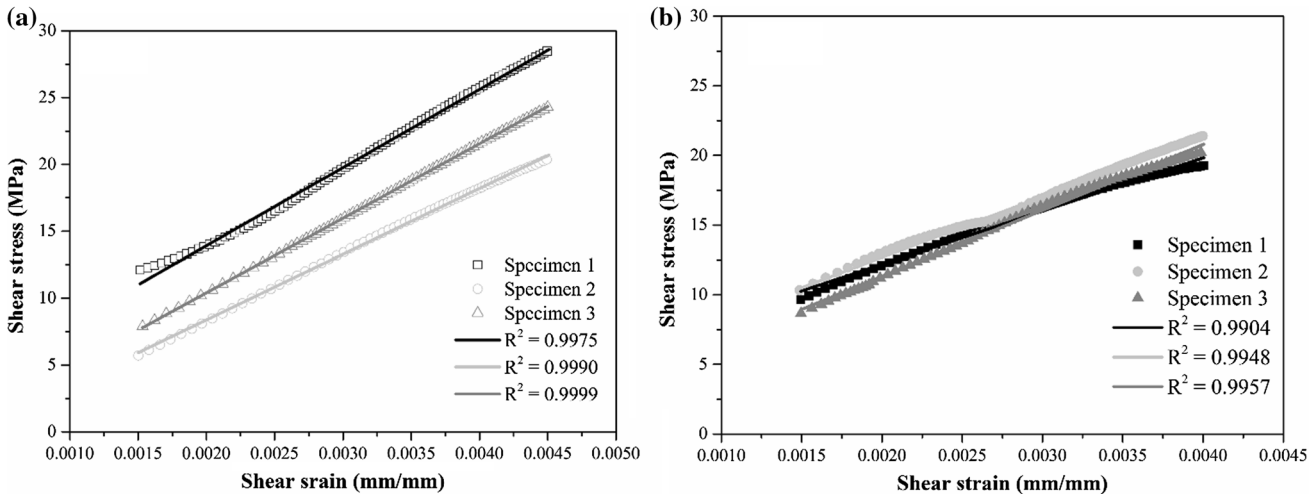

Fig. 14 Shear stress × strain curves for non-aged **a** and aged **b** specimens for the determination of shear modulus

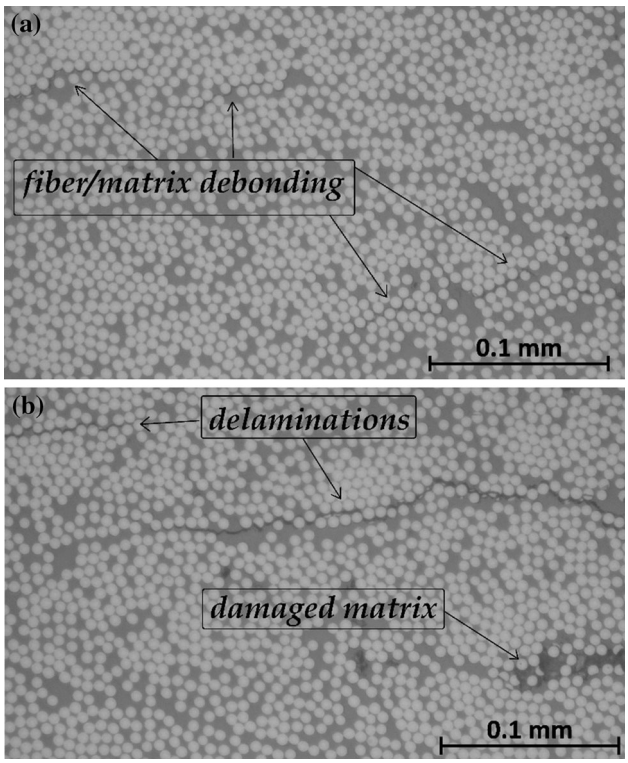

Fig. 15 Representative optical micrographs from the non-aged **a** and aged **b** $[0]_4$ tested shear specimens

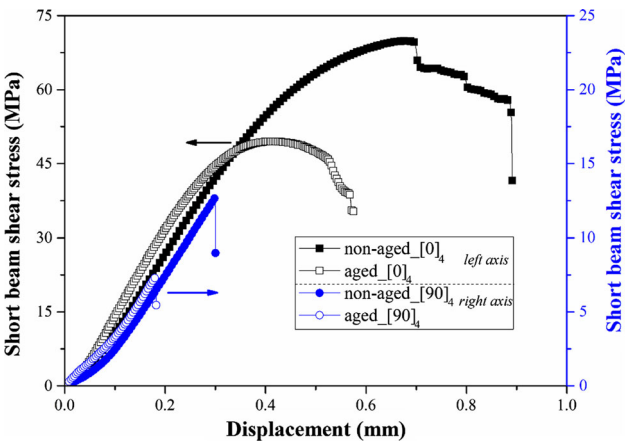

Fig. 16 Short beam stress versus displacement for all family of laminates studied

Even though shear is the dominant loading in this test, the internal stress state is complex and a variety of failure modes can occur, such as interlaminar shear, micro-buckling, flexure, tension, compression, or their combination. In this test, the maximum shear stress occurs in a region where other stresses might also exist [25] and stress distribution may be distorted, with peak stresses taking place close to the loading points, even if the recommended span-to-thickness ratio of 4:1 [26] was used. Also, the local stress state due to the applied load may involve several shear-stress concentrations combined with transverse and in-plane compressive stresses.

Figure 17 presents representative SEM images for the unconditioned 0° and 90° coupons. Failure in both 0° specimens was as expected, that is, large delamination at the mid-plane of the specimen thickness and multiple translaminar horizontal cracks, characterizing interlaminar shear failure [25, 27]. On the other hand, both 90° specimens showed a matrix-dominated failure and did not present evidence of shear failure. Indeed, a vertical crack initiated at the specimen bottom surface between the supporting cylinders, characterizing failure by flexure and primarily transverse tensile, justified by the brittle behavior of epoxy and fiber orientation. Compressive failure was not noticed.

The achieved material properties are compiled in Table 2. The data presented low scatter in general, which is attributed to the advanced and automated manufacturing process used and the laminate consolidation by hot compression prior to curing. The final laminates were nearly free of voids, as confirmed by optical and SEM micrographs. Reduction in all properties was noticed for the aged laminates due to the aforementioned reasons.

Failure envelopes

Failure envelopes for both non-aged and aged laminates were produced, based on several failure criteria as shown in Fig. 18, in σ_{22}–τ_{12} plane. In most cases, matrix failure implies catastrophic failure of the laminate. In those cases, ultimate failure stress and strain of the laminates are the stress/strain corresponding to matrix failure [27].

For the maximum stress failure criteria, there is no shear. For all other criteria, shear stresses are taken into account, being more theoretically accurate for a case in which the σ_{22}–τ_{12} plane is under study. Under tensile stress, all failure criteria tend to produce similar values due to the low magnitude of the transverse tensile strength of the unidirectional laminate. However, for the combination of transverse compression and in-plane shear, the envelopes present different predictions. In particular, the Puck criterion can be related to the previous optical and SEM results, since it suggests angular fracture for the specimens under compressive loading due to a combination of micro-buckling, compression, and shear forces, typical of the Mode B inter-fiber failure. In addition, for the in-plane shear tests, delaminations, fiber/matrix debonding, and interlaminar fractures were reported, being characteristic of the Mode C inter-fiber failure in Puck criterion.

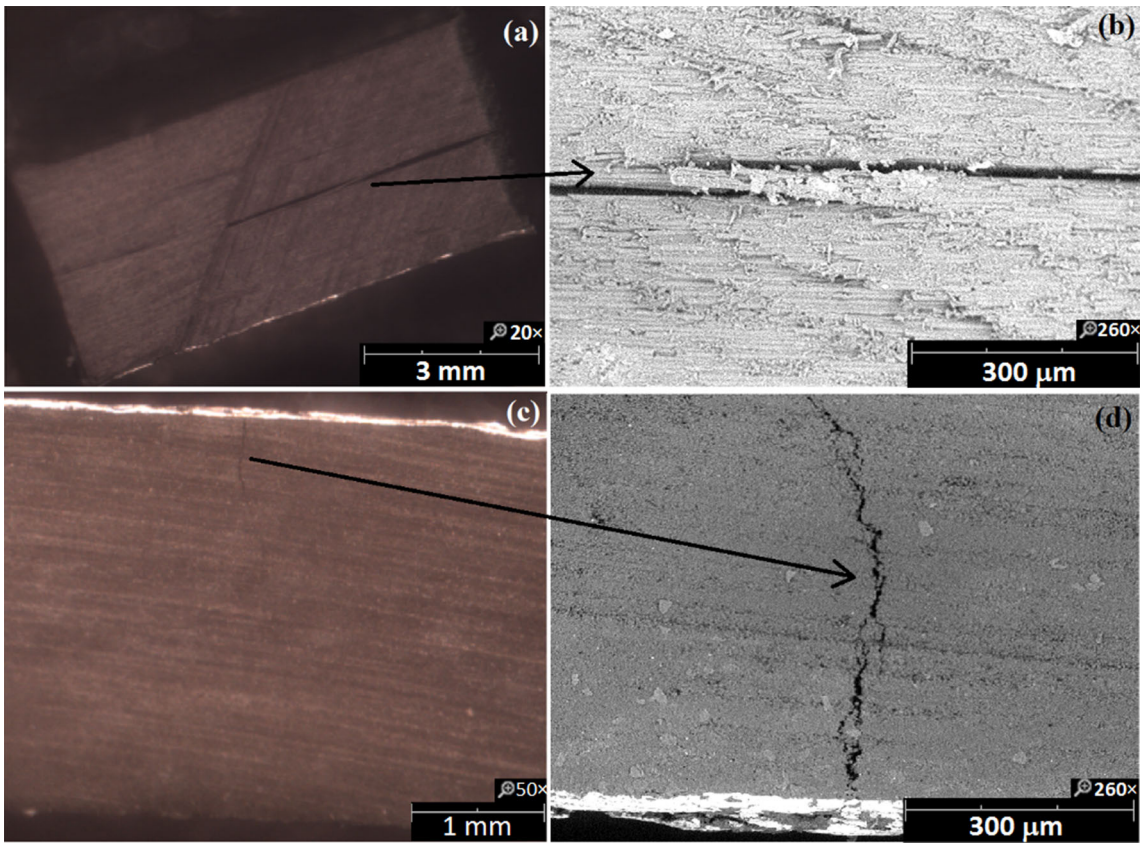

Fig. 17 SEM micrographs of the fractured short beam specimens: non_aged_$[0]_4$ (**a**) with a zoom at the delamination (**b**), and non_aged_$[90]_4$ (**c**) with a zoom at the crack (**d**)

Table 2 Summary of the measured properties

Elastic	Non-aged	Aged	Variation	Strength	Non-aged	Aged	Variation (%)
$E_{1,t} = E_{1,c}$ (GPa)	129.3 ± 3.6	119.7 ± 4.1	↓7 %	X_t (MPa)	1409.9 ± 131.6	1091.0 ± 114.0	↓23
$E_{2,t} = E_{2,c}$ (GPa)	9.11 ± 0.49	6.3 ± 0.8	↓31 %	Y_t (MPa)	42.5 ± 3.2	31.8 ± 1.2	↓25
G_{12} (GPa)	5.44 ± 0.48	3.89 ± 0.19	↓28 %	X_c (MPa)	764.1 ± 79.6	621.2 ± 81.0	↓19
				Y_c (MPa)	134.5 ± 7.8	121.6 ± 9.8	↓10
ν_{12}	0.322 ± 0.023	0.331 ± 0.011	↑3 %	S_{12} (MPa)	68.9 ± 5.1	41.4 ± 4.0	↓40
				SBS $[0]_4$ (MPa)	69.9 ± 1.1	49.5 ± 1.3	↓29
ν_{21}	0.022*	0.029*	–	SBS $[90]_4$ (MPa)	12.6 ± 0.6	7.4 ± 0.7	↓41

* Calculated

Conclusions

In this work, the effect of weathering on tensile, compressive, in-plane shear, interlaminar, and viscoelastic properties of flat carbon fiber/epoxy composites manufactured by FW were evaluated. The composite coupons were subjected to an accelerated hygrothermal conditioning for 60 days under 80 °C and relative humidity of 90 %. Moisture absorption achieved a maximum of 0.42 % in weight, with saturation at around 33 days. Non-Fickian kinetics was found to govern moisture absorption in the final stages of weathering probably due to the leaching of low-molecular weight molecules. Matrix plasticization and a strong variation in T_g with aging were also noticed, the lowest T_g being found for the conditioned 90° specimen.

Regarding mechanical properties, both tensile and compressive strength/modulus values were found to decrease for aged laminates, as well as the Poisson's ratio. The 90° specimens were more strongly affected by aging, since a matrix-dominated failure is expected in this direction. Mean shear modulus and strength reduced in as much as 30 and 40 %, respectively, and the dominant failure mode of the V-notched specimens was primarily fiber/matrix debonding and delaminations. Short beam tests

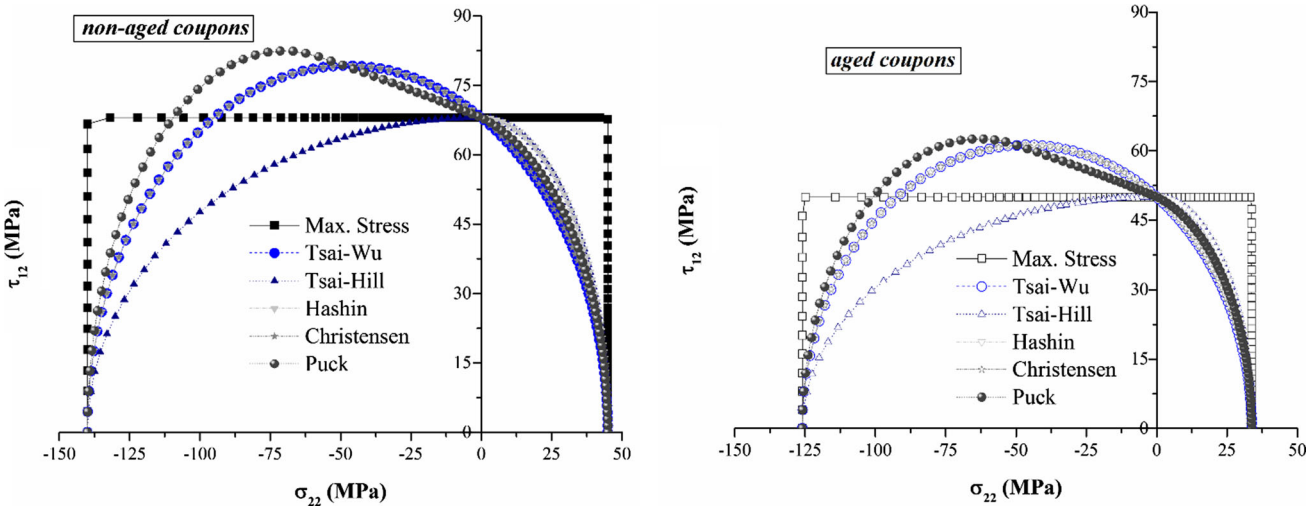

Fig. 18 Failure envelopes for both non-aged and aged composite laminates for several failure criteria considering $\sigma_{11} = 0$

were considered successful since the specimens failed by interlaminar shear, with large delaminations and multiple horizontal cracks throughout the specimen half-thickness for the 0^{o} laminates.

The fractographic analyses justified the strong effect noticed on matrix-dominated properties due to the degradation of the epoxy matrix. This degradation led to a subsequent decrease in interfacial strength, which dominated the reduction in shear properties. Based on the fractographic analyses and the estimates, the Puck's failure criterion was found more accurate, B and C being inter-fiber fracture modes dominant for the studied laminates.

Acknowledgements The authors would like to thank CAPES, FAPESP, CNPq, and AEB (Brazilian Space Agency) for the financial support.

References

1. Botelho EC, Costa ML, Pardini LC, Rezende MC (2005) Processing and hygrothermal effects on viscoelastic behavior of glass fiber/epoxy composites. J Mater Sci 40(14):3615–3623. doi:10.1007/s10853-005-0760-2
2. Almeida JHS Jr, Faria H, Marques AT, Amico SC (2014) Load sharing ability of the liner in type III composite pressure vessels under internal pressure. J Reinf Plast Compos 33(24):2274–2286
3. Pillay S, Vaidya UK, Janowski GM (2009) Effects of moisture and UV exposure on liquid molded carbon fabric reinforced nylon 6 composite laminates. Compos Sci Technol 69(6):839–846
4. Bao L-R, Yee AF (2002) Moisture diffusion and hygrothermal aging in bismaleimide matrix carbon fiber composites: part II-Woven and hybrid composites. Compos Sci Technol 62(16):2111–2119
5. Zhang A, Lu H, Zhang D (2014) Synergistic effect of cyclic mechanical loading and moisture absorption on the bending fatigue performance of carbon/epoxy composites. J Mater Sci 49(1):314–320. doi:10.1007/s10853-013-7707-9
6. Zheng Q, Morgan RJ (1993) Synergistic thermal-moisture damage mechanisms of epoxies and their carbon fiber composites. J Compos Mater 27(15):1465–1478
7. Bao L-R, Yee AF (2002) Effect of temperature on moisture absorption in a bismaleimide resin and its carbon fiber composites. Polymer 43(14):3987–3997
8. Kumar BG, Singh RP, Nakamura T (2002) Degradation of carbon fiber-reinforced epoxy composites by ultraviolet radiation and condensation. J Comp Mater 36(24):2713–2733
9. Mouzakis DE, Zoga H, Galiotis C (2008) Accelerated environmental aging study of polyester/glass fiber reinforced composites (GFRPCs). Compos B 39(3):467–475
10. Batista NL, Faria MCM, Iha K, Oliveira PC, Botelho EC (2015) Influence of water immersion and ultraviolet weathering on mechanical and viscoelastic properties of polyphenylene sulfide–carbon fiber composites. J Thermoplast Compos Mater 28(3):340–356
11. Botelho EC, Pardini LC, Rezende MC (2006) Hygrothermal effects on the shear properties of carbon fiber/epoxy composites. J Mater Sci 41(21):7111–7118. doi:10.1007/s10853-006-0933-7
12. Tsai YI, Bosze EJ, Barjasteh E, Nutt SR (2009) Influence of hygrothermal environment on thermal and mechanical properties of carbon fiber/fiberglass hybrid composites. Compos Sci Technol 69(3–4):432–437
13. Sun P, Zhao Y, Luo Y, Sun L (2011) Effect of temperature and cyclic hygrothermal aging on the interlaminar shear strength of carbon fiber/bismaleimide (BMI) composite. Mater Des 32(8–9):4341–4347
14. Tsai SW, Wu EM (1971) A general theory of strength for anisotropic materials. J Compos Mater 5(1):58–80
15. Tsai SW (1965) Strength characteristics of composite materials, NASA technical report CR-224
16. Hashin Z (1979) Analysis of properties of fiber composites with anisotropic constituents. J Appl Mech 46(3):543–550
17. Christensen RM (1997) Stress based yield/failure criteria for fiber composites. Int J Solid Struct 34(5):529–543
18. Puck A, Mannigal M (2007) Physically based non-linear stress-strain relations for the inter-fiber fracture analysis of FRP laminates. Compos Sci Technol 67(9):1955–1964
19. Karbhari VM, Xian G (2009) Hygrothermal effects on high V_F pultruded unidirectional carbon/epoxy composites: moisture uptake. Compos B 40(1):41–49
20. Jiang X, Kolstein H, Bijlaard F, Qiang X (2014) Effects of hygrothermal aging on glass-fibre reinforced polymer laminates and adhesive of FRP composite bridge: moisture diffusion characteristics. Compos A 57:49–58
21. Chandra R, Singh SP, Gupta K (1999) Damping studies in fibre-reinforced composites—a review. Compos Struct 46(1):41–51

22. Nakanishi Y, Hana K, Hamada H (1997) Fractography of fracture in CFRP under compressive load. Compos SciTechnol 57(8):1139–1147
23. Pinho ST, Iannucci L, Robinson P (2006) Physically-based failure models and criteria for laminated fibre-reinforced composites with emphasis on fibre kinking: part I: Development. Compos A 37(1):63–73
24. Almeida JHS Jr, Angrizani CC, Botelho EC, Amico SC (2015) Effect of fiber orientation on the shear behavior of glass fiber/epoxy composites. Mater Des 65:789–795
25. Whitney JM, Browning CE (1985) On short-beam shear tests for composite materials. Exp Mech 25(3):294–300
26. Silva LV, Júnior JHSA, Angrizani CC, Amico SC (2013) Short beam strength of curaua, sisal, glass and hybrid composites. J Reinf Plast Compos 32(3):197–206
27. Sun CT, Tao J (1998) Prediction of failure envelopes and stress/strain behaviour of composite laminates. Compos Sci Technol 58(7):1125–1136